Photoelectrochemistry

International Edition: DOI: 10.1002/anie.201410944
German Edition: DOI: 10.1002/ange.201410944

Electro-assembly of a Chromophore–Catalyst Bilayer for Water Oxidation and Photocatalytic Water Splitting**

*Dennis L. Ashford, Benjamin D. Sherman, Robert A. Binstead, Joseph L. Templeton, and Thomas J. Meyer**

Abstract: *The use of electropolymerization to prepare electrocatalytically and photocatalytically active electrodes for water oxidation is described. Electropolymerization of the catalyst Ru^{II}(bda)(4-vinylpyridine)$_2$ (bda = 2,2′-bipyridine-6,6′-dicarboxylate) on planar electrodes results in films containing semirigid polymer networks. In these films there is a change in the water oxidation mechanism compared to the solution analogue from bimolecular to single-site. Electro-assembly construction of a chromophore–catalyst structure on mesoporous, nanoparticle TiO_2 films provides the basis for a dye-sensitized photoelectrosynthesis cell (DSPEC) for sustained water splitting in a pH 7 phosphate buffer solution. Photogenerated oxygen was measured in real-time by use of a two-electrode cell design.*

Water oxidation to oxygen is the crucial "other" half reaction in solar water splitting and CO_2 reduction to reduced forms of carbon. An important development has been the discovery of the complexes Ru^{II}(bda)(L)$_2$ (H_2bda = 2,2′-bipyridine-6,6′-dicarboxylic acid; L is a neutral donor ligand) by Sun and co-workers. They report high catalytic water oxidation rates and turnover numbers in acidic solutions with Ce^{IV} as the oxidant.[1]

In electrocatalytic and photoelectrocatalytic applications, stable surface immobilization on high band gap oxide semiconductors is a key element. Electropolymerization enables an "on-surface" preparation of assemblies by electrochemically induced C–C bond coupling.[2] This technique has been applied to the preparation of films of the vinyl-functionalized complex, Ru(bda)(4-vinylpyridine)$_2$ (**1**), on both glassy carbon and metal oxide electrodes for electrocatalytic water oxidation and, in a bilayer chromophore–catalyst assembly on metal oxides, for use in a dye-sensitized photoelectrosynthesis cell (DSPEC) for water splitting.

Structures of the phosphonate-derivatized, light-harvesting chromophore $[Ru(dvb)_2((PO_3H_2)_2bpy)]^{2+}$ ($RuPdvb^{2+}$; dvb = 5,5′-divinyl-2,2′-bipyridine; $(PO_3H_2)_2$bpy = [2,2′-bipyridine]-4,4′-diylbis(phosphonic acid)), the vinyl-functionalized molecular water oxidation catalyst **1**, and the solution analogue Ru(bda)(4-picoline)$_2$ (**2**) are shown in Figure 1 A.[2a,b]

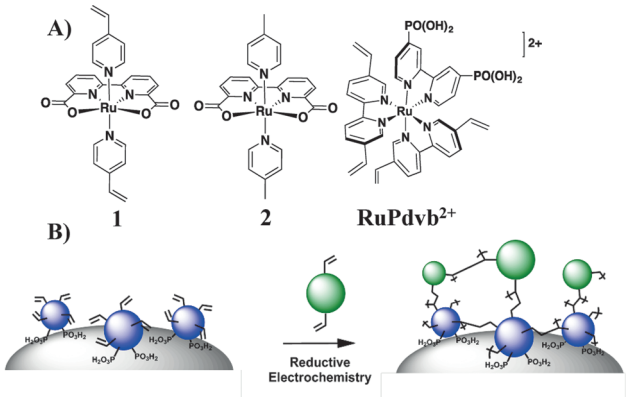

Figure 1. A) Structures of **1**, **2**, and $RuPdvb^{2+}$. B) Schematic diagram of the surface structure following reductive electropolymerization of **1** on TiO_2-$RuPdvb^{2+}$.

To investigate film-based water oxidation reactivity, **1** was electropolymerized on glassy carbon (GC), to give GC-poly**1**, by chronocoulometry with the working electrode held initially at −2.4 V (vs. $Ag/AgNO_3$) for 1 s followed by 0 V (vs. $Ag/AgNO_3$) for 10 seconds. Surface coverages (Γ), determined by the integrated charge under the $Ru^{III/II}$ wave in cyclic voltammograms and Equation (S1), were linear with the number of potential-step cycles (Figure S4). All experiments for GC-poly**1** were carried out following 80 cycles of electrodeposition. The peak current (i_p) for the poly$Ru^{III/II}$ redox couple in aqueous 0.1 M $HClO_4$ varied linearly with scan rate on GC-poly**1** (Figure S5), consistent with a nondiffusional surface redox couple.[3]

The pH dependence of the redox couples for **2** in aqueous 30% CF_3CH_2OH (TFE) and in 4% CH_3CN have been previously reported.[1b,4] There is experimental evidence that the Ru^{II} form of **2** in 30% TFE is symmetric with both carboxylate arms coordinated whereas CH_3CN is bound with 4% added CH_3CN.[4] Coordination of CH_3CN is also observed in poly**1** as shown by the ca. 200 mV positive shift

[*] Dr. D. L. Ashford, Dr. B. D. Sherman, Dr. R. A. Binstead, Prof. J. L. Templeton, Prof. T. J. Meyer
Department of Chemistry
University of North Carolina at Chapel Hill
Chapel Hill, North Carolina 27599, United States
E-mail: tjmeyer@unc.edu

[**] This research was supported by the UNC EFRC Center for Solar Fuels, an Energy Frontier Research Center funded by the U.S. Department of Energy, Office of Science, Office of Basic Energy Sciences, under Award No. DE-SC0001011, supporting B.D.S. and R.A.B. D.L.A. acknowledges support from the Department of Energy Office of Science Graduate Fellowship Program under Contract No. DE-AC05-06OR23100.

Supporting information for this article (including detailed experimental procedures, synthetic preps, electrochemical characterization, and photoelectrochemical analysis) is available on the WWW under http://dx.doi.org/10.1002/anie.201410944.

in the $Ru^{III/II}$ redox couple following addition of 4% CH_3CN in aqueous 0.1 M $HClO_4$ (Figure S6).

The results of pH-dependent electrochemical studies on GC-poly**1** in both 30% TFE and 4% CH_3CN are summarized in the $E_{1/2}$ ($\approx E^{0\prime}$; $E^{0\prime}$ is the formal potential) versus pH (Pourbaix) diagrams shown in Figure 2. In 30% TFE, the

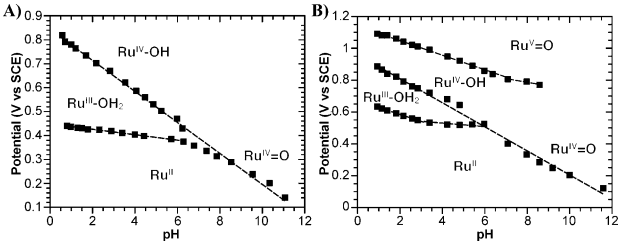

Figure 2. Pourbaix ($E_{1/2}$ vs. pH) diagram for GC-poly**1** in aqueous 30% CF_3CH_2OH (TFE) (A) and 4% CH_3CN (B) in 0.12 M Britton–Robinson buffer in 0.5 M $NaClO_4$. $E_{1/2}$ values were obtained from square wave voltammograms.

$Ru^{III/II}$ couple is pH-independent up to about pH 6, consistent with an oxidation to Ru^{III} followed by subsequent coordination of water, -Ru^{II} $\xrightarrow{-e^-,+H_2O}$ -Ru^{III}-OH_2^+ with p$K_a \approx 6$ for -Ru^{III}-OH_2^+.[1b,4] The non-zero slope (≈ -10 mV/pH unit) for the $Ru^{III/II}$ couple at pH < 6 is a general observation for nominally pH-independent couples on electrode surfaces as noted earlier.[5] The -$Ru^{IV/III}$ redox couple is pH-dependent from pH 0.5 to 11 (≈ -64 mV/pH unit) with a dependence consistent with p$K_a \approx 6$ for -Ru^{IV}-OH^+ as reported earlier.[1b,4] At pH > 6, -Ru^{III}-OH, is unstable with respect to disproportionation, and only the $Ru^{IV/II}$ redox couple is observed. A -$Ru^{V/IV}$ redox couple was not observed at any pH in 30% TFE.

With 4% added CH_3CN, the Pourbaix diagram (Figure 2) for GC-poly**1** is similar to the diagram in 30% TFE, but with a positive shift of ca. 200 mV in the -$Ru^{III/II}$ couple due to coordination of CH_3CN.[1b] Following oxidation to Ru^{III}, the nitrile ligand is replaced by water.[4] In contrast to 30% TFE, the -$Ru^{V/IV}$ couple is observable in 4% CH_3CN. The pK_a values for -Ru^{III}-OH_2^+ and -Ru^{IV}-OH^+ are around 6 in this medium, comparable to the values in 30% TFE and for **2** in solution.[1b]

Cyclic voltammograms for the solution catalyst, **2**, were recorded at pH 1, 4, and 7 in both 30% TFE and 4% CH_3CN for comparison with GC-poly**1**. In solution, the $Ru^{III/II}$ wave is similar to the wave for the $Ru^{III/II}$ couple on GC-poly**1** under all conditions. The $Ru^{IV/III}$ couple is kinetically inhibited for GC-poly**1**, but the $E_{1/2}$ value appears at a similar potential in both media (Figures 3, S7, and S8). In contrast, the onset for catalytic water oxidation by **2** in solution occurs at a lower potential than for GC-poly**1** in both media. The shifts to lower potential by about 250 mV points to a change in mechanism on the surface compared to solution.[1b]

As noted above, based on the results of kinetic and mechanistic studies, it has been proposed that water oxidation by **2** involves rate-limiting, bimolecular O–O bond formation following oxidation to Ru^V.[1a,b] In the semirigid polymer network, poly**1** is immobilized so that a bimolecular pathway

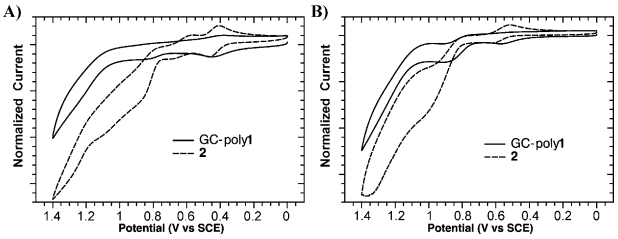

Figure 3. Cyclic voltammograms (CVs) for GC-poly**1** (solid) and **2** (dashed) in 0.1 M phosphate, 0.5 M $NaClO_4$ at pH 7 with: A) 30% TFE added, and B) 4% CH_3CN added: 50 mV s^{-1}, 23 °C, Pt-wire counter, and SCE reference electrode. CVs were normalized to the $Ru^{III/II}$ couple for comparison purposes.

is greatly inhibited and water oxidation is expected to be dominated by a single-site mechanism or mechanisms.[6] Single-site catalysis is supported by the results of a surface dilution experiment with poly**1** copolymerized with [Fe(4′-(4-vinylphenyl)-2,2′:6′,2″-terpyridine)$_2$]$^{2+}$ (Fe(v-trpy)$_2^{2+}$) in a 65:35 poly**1**:poly(Fe(v-trpy)$_2^{2+}$ ratio.[2b] As shown in Figure 4, when normalized for the amount of catalyst in the film, there was no sign of inhibition of water oxidation catalysis in the mixed film.

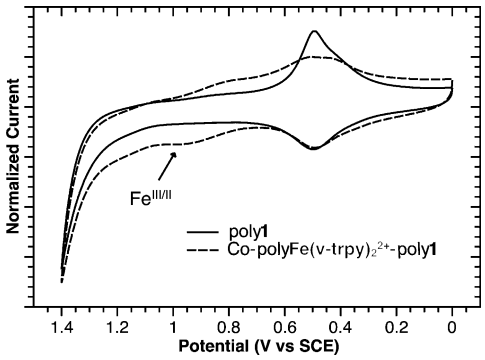

Figure 4. Cyclic voltammograms of GC-poly**1** (solid) and copolymer film GC-poly**1**-polyFe(v-trpy)$_2^{2+}$ (dashed) with ≈35% Fe(v-trpy)$_2^{2+}$ incorporated into the film (scan rate 50 mV s^{-1}, Pt-wire counter, and SCE reference electrode). CVs were normalized to the $Ru^{III/II}$ redox couple for comparison purposes. The film was generated by first holding the potential at −2.4 V (vs. Ag/$AgNO_3$) for 1 s then at 0 V (vs. Ag/$AgNO_3$) for 10 s, followed by holding at −1.8 V (vs. Ag/$AgNO_3$) for 1 s and finally at 0 V for 10 s. This cycle was repeated 100 times to build the copolymer film GC-poly**1**-polyFe(v-trpy)$_2^{2+}$.

Water oxidation by GC-poly**1** was further evaluated at a rotating ring-disk electrode (RRDE) at both pH 1 (0.1 M $HClO_4$ with 0.4 M $NaClO_4$) and pH 7 (0.1 M phosphate buffer (0.061 M HPO_4^{2-}) with 0.4 M $NaClO_4$) at room temperature.[7] Figure 5 shows characteristic linear sweep voltammograms collected with a glassy carbon disk and platinum ring electrode for the GC surface modified with poly**1** and, for comparison, a polished GC surface without catalyst. The onset of catalytic current near 0.95 V versus SCE is matched by an increase in cathodic current at the platinum ring (held at −0.45 V vs. SCE) consistent with the generation of O_2 by poly**1**.[7a] Based on the RRDE results, Faradaic efficiencies for

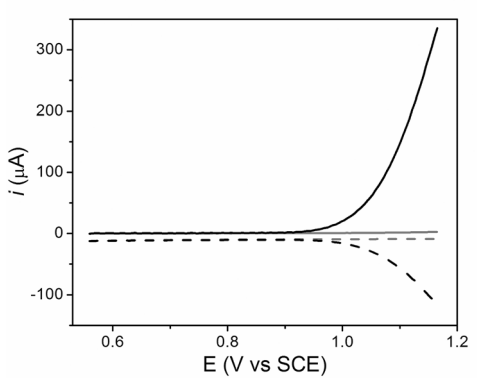

Figure 5. RRDE linear sweep voltammogram with a GC disk electropolymerized with poly**1** (black, ≈5 monolayers of poly**1**) in 0.1 M phosphate buffer at pH 7 with 0.4 M $NaClO_4$. The corresponding chronoamperometric trace at the Pt ring (black dash) is also shown as is the background current observed with a polished GC disk (grey) and Pt ring (grey dash). Linear voltammograms were recorded at a scan rate of 5 $mV s^{-1}$ with an electrode rotation rate of 500 RPM. The Pt ring was held at −0.45 V versus SCE. The currents measured at the Pt ring are corrected for the collection efficiency of the ring-disk electrode assembly (23%) determined independently.

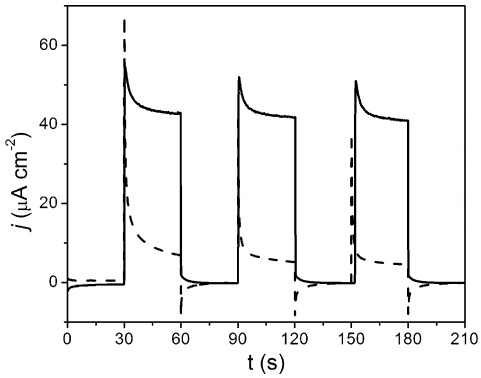

Figure 6. Photocurrent traces with 30 second light off/on cycles for (solid) $n$$TiO_2$-RuPdvb^{2+}-poly**1** held at a bias of 0.2 V versus SCE and (dashed) $n$$TiO_2$-RuPdvb^{2+} under the same bias (0.2 V versus SCE). The electrolyte contained 0.1 M phosphate buffer at pH 7 with 0.4 M $NaClO_4$ and 100 $mW cm^{-2}$ (380 nm long-pass filter) illumination was used during illuminated cycles.

O_2 production were 62% and 13% at pH 7 and 1, respectively. There may be competing anodic processes that dominate in acidic solution. The observed efficiencies are comparable to those observed earlier for a Ru-based catalyst also studied by RRDE.[7a] A comparable experiment, shown in Figure S9, but with the Pt ring held at 0.065 V versus SCE, failed to provide evidence for H_2O_2 (Figure S9).

Turnover frequencies (TOF) for O_2 production were also determined by RRDE measurements using the current arising from O_2 reduction. At pH 7 with added $H_2PO_4^-$/HPO_4^{2-} buffer ($[HPO_4^{2-}] = 0.061$M), the TOF for O_2 production was 8.5 mol O_2/mol poly**1** s^{-1} at an applied bias of 1.2 V versus SCE, an overvoltage (η) of 620 mV. The same analysis at pH 1 gave a TOF of 0.047 mol O_2/mol poly**1** s^{-1} with an applied bias of 1.6 V versus SCE ($\eta = 670$ mV). The enhancement with added $H_2PO_4^-$/HPO_4^{2-} is an expected result, arising from the intervention of atom-proton transfer (APT) pathways with HPO_4^{2-} dominating as a proton acceptor during O–O bond formation.[8]

With the ability of poly**1** to act as a water oxidation catalyst in polymerized films, we turned to the electroassembly formation of the chromophore–catalyst RuPdvb^{2+}-poly**1** on nanocrystalline TiO_2 ($n$$TiO_2$). The assembly, which is illustrated schematically in Figure 1 B, was prepared by prior surface binding of RuPdvb^{2+} ($n$$TiO_2$-RuPdvb^{2+}) followed by electrodeposition of **1**. In these experiments, RuPdvb^{2+} was preloaded on ca. 5 μm thick, nanocrystalline films of TiO_2 on fluorine-doped tin oxide (FTO). Following 60 reductive cycles in a 0.5 mM solution of **1** in propylene carbonate 0.1M in $TBAPF_6$, a 1:1 overlayer of poly**1** ($\Gamma \approx 7 \times 10^{-8}$ mol cm^{-2}) was determined by UV/Vis measurements.[2a,b] The $n$$TiO_2$-RuPdvb^{2+}-poly**1** electrodes showed significantly higher sustained photocurrents than the control $n$$TiO_2$-RuPdvb^{2+} electrodes indicating sustained photodriven water oxidation catalysis (Figure 6)

As shown in Figure 7, stable photocurrents were obtained with white light illumination (100 $mW cm^{-2}$, 380 nm long-pass filter) of the $n$$TiO_2$-RuPdvb^{2+}-poly**1** photoanode over 10 min periods. The experiments were carried out in a DSPEC configuration with a separate Pt cathode for H_2 production in 0.1M phosphate buffer at pH 7 (0.4 M $NaClO_4$ supporting electrolyte) with a 0.2 V (vs. SCE) applied bias. O_2 production from the photoanode was verified by a dual working electrode technique modified from a method described earlier by Mallouk and co-workers.[9] As shown in Figure 7, upon illumination of $n$$TiO_2$-RuPdvb^{2+}-poly**1** with sustained anodic photocurrent, O_2 reduction is observed at the second, FTO working electrode. At the end of the photolysis period, the cathodic current for O_2 reduction at the FTO electrode begins to decrease and eventually reaches the baseline. Comparison of the charge passed at the FTO from the reduction of O_2 and that passed during the illumination of the $n$$TiO_2$-RuPdvb^{2+}-

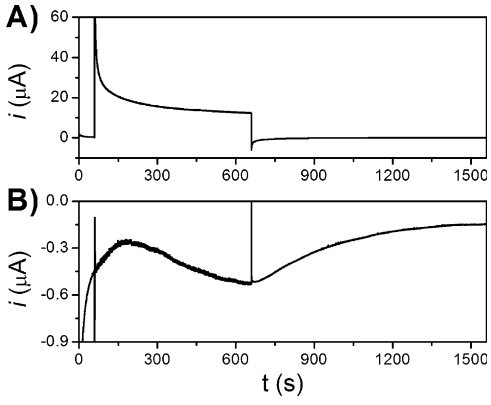

Figure 7. Upper pane: A) current–time trace (60–600 s) at illuminated (100 $mW cm^{-2}$, 380 nm long-pass filter) $n$$TiO_2$-RuPdvb^{2+}-poly**1** in 0.1 M phosphate buffer 0.4 M in $NaClO_4$ at an applied bias of 0.2 V versus SCE. Lower pane: B) current trace measured at an FTO electrode ca. 1 mm from $n$$TiO_2$-RuPdvb^{2+}-poly**1** at an applied bias of −0.8 V versus SCE concurrently with the photoelectrochemical trace, see SI for details.

poly**1** photoanode gives a faradaic efficiency of 8% for O_2 production under 1 sun illumination (100 mW cm^{-2}, additional details provided in the Supporting Information, SI).

Similar chromophore–catalyst systems have recently been reported for use in a DSPEC.[10] The photocurrent densities observed here are comparable to previous reports,[10d,e] and modest in comparison with others.[10a,b] Differences in illumination intensities and electrode thicknesses used across these studies, in part, explains the variation in observed photocurrents. However, it is important to note, that the electropolymerization strategy of immobilization results in a change in the mechanism from bimolecular[1a–c] to a single-site mechanism, and with it, the catalytic rates. This is important in understanding the mechanism of this family of catalysts and future design principles.

Our results are important in extending the electropolymerization/electro-assembly strategy to water oxidation in films and on oxide surfaces by water oxidation catalyst **1**. The coordination chemistry and PCET properties of **2** in solution are maintained for **1** in the electropolymerized films although the film environment does enforce a single-site mechanism for the O–O bond-forming step. Prior surface binding of $RuPdvb^{2+}$ followed by electro-assembly formation with **1** in the external solution provides a route to the photoanode *n*TiO_2-$RuPdvb^{2+}$-poly**1** and a basis for sustained DSPEC water splitting. This proves the electropolymerized technique explored here is a viable means of preparing photocatalytically active surfaces on metal oxide electrodes. Experiments in progress are exploring core–shell strategies and varying chromophore/catalyst ratios to maximize efficiencies for water splitting and gain long-term stability of the vinyl-coupled assemblies.

Keywords: electropolymerization · photoelectrochemistry · proton-coupled electron transfer · solar fuels · water oxidation

How to cite: *Angew. Chem. Int. Ed.* **2015**, *54*, 4778–4781
Angew. Chem. **2015**, *127*, 4860–4863

[1] a) L. Duan, C. M. Araujo, M. S. G. Ahlquist, L. Sun, *Proc. Natl. Acad. Sci. USA* **2012**, *109*, 15584–15588; b) L. Duan, F. Bozoglian, S. Mandal, B. Stewart, T. Privalov, A. Llobet, L. Sun, *Nat. Chem.* **2012**, *4*, 418–423; c) L. Duan, A. Fischer, Y. Xu, L. Sun, *J. Am. Chem. Soc.* **2009**, *131*, 10397–10399; d) L. Duan, L. Wang, A. K. Inge, A. Fischer, X. Zou, L. Sun, *Inorg. Chem.* **2013**, *52*, 7844–7852.

[2] a) D. L. Ashford, A. M. Lapides, A. K. Vannucci, K. Hanson, D. A. Torelli, D. P. Harrison, J. L. Templeton, T. J. Meyer, *J. Am. Chem. Soc.* **2014**, *136*, 6578–6581; b) A. M. Lapides, D. L. Ashford, K. Hanson, D. A. Torelli, J. L. Templeton, T. J. Meyer, *J. Am. Chem. Soc.* **2013**, *135*, 15450–15458; c) N. Oyama, F. C. Anson, *J. Am. Chem. Soc.* **1979**, *101*, 3450–3456; d) H. D. Abruña, *Coord. Chem. Rev.* **1988**, *86*, 135–189.

[3] A. J. Bard, L. R. Faulkner, *Electrochemical Methods: Fundamentals and Applications*, 2nd ed., Wiley, New York, **2001**.

[4] N. Song, J. J. Concepcion, R. A. Binstead, J. A. Rudd, A. K. Vannucci, C. Dares, T. J. Meyer, unpublished results.

[5] a) D. L. Ashford, W. J. Song, J. J. Concepcion, C. R. K. Glasson, M. K. Brennaman, M. R. Norris, Z. Fang, J. L. Templeton, T. J. Meyer, *J. Am. Chem. Soc.* **2012**, *134*, 19189–19198; b) S. G. Yan, J. T. Hupp, *J. Phys. Chem.* **1996**, *100*, 6867–6870; c) A. Zaban, S. Ferrere, B. A. Gregg, *J. Phys. Chem. B* **1998**, *102*, 452–460.

[6] J. J. Concepcion, J. W. Jurss, J. L. Templeton, T. J. Meyer, *J. Am. Chem. Soc.* **2008**, *130*, 16462–16463.

[7] a) J. J. Concepcion, R. A. Binstead, L. Alibabaei, T. J. Meyer, *Inorg. Chem.* **2013**, *52*, 10744–10746; b) T. Nakagawa, N. S. Bjorge, R. W. Murray, *J. Am. Chem. Soc.* **2009**, *131*, 15578–15579.

[8] Z. F. Chen, J. J. Concepcion, X. Q. Hu, W. T. Yang, P. G. Hoertz, T. J. Meyer, *Proc. Natl. Acad. Sci. USA* **2010**, *107*, 7225–7229.

[9] S.-H. A. Lee, Y. Zhao, E. A. Hernandez-Pagan, L. Blasdel, W. J. Youngblood, T. E. Mallouk, *Faraday Discuss.* **2012**, *155*, 165–176.

[10] a) Y. Gao, X. Ding, J. Liu, L. Wang, Z. Lu, L. Li, L. Sun, *J. Am. Chem. Soc.* **2013**, *135*, 4219–4222; b) Y. Gao, L. Zhang, X. Ding, L. Sun, *Phys. Chem. Chem. Phys.* **2014**, *16*, 12008–12013; c) X. Ding, Y. Gao, L. Zhang, Z. Yu, J. Liu, L. Sun, *ACS Catal.* **2014**, *4*, 2347–2350; d) X. Ding, Y. Gao, L. Zhang, Z. Yu, J. Liu, L. Sun, *Electrochim. Acta* **2014**, *149*, 337–340; e) T.-T. Li, W.-L. Zhao, Y. Chen, F.-M. Li, C.-J. Wang, Y.-H. Tian, W.-F. Fu, *Chem. Eur. J.* **2014**, *20*, 13957–13964.

Received: November 11, 2014
Revised: December 15, 2014
Published online: February 23, 2015

